separations

MDPI

Article

In Situ N-Doped Low-Corrosion Porous Carbon Derived from Biomass for Efficient CH_4/N_2 Separation

Huihui Wang [1], Yuqiong Zhao [1,*], He Lian [1], Qi Wang [2], Zhihong Shang [3] and Guojie Zhang [1,*]

[1] State Key Laboratory of Clean and Efficient Coal Utilization, Taiyuan University of Technology, Taiyuan 030024, China
[2] Department of Basic Sciences, Shanxi Agricultural University, Jinzhong 030801, China
[3] Jinneng Holding Group Co., Ltd., Taiyuan 030006, China
* Correspondence: zhaoyuqiong@tyut.edu.cn (Y.Z.); zhangguojie@tyut.edu.cn (G.Z.)

Abstract: The separation of CH_4 and N_2 is essential for the effective use of low-concentration coalbed methane (CBM). In this study, a series of nitrogen-doped porous carbons were synthesized using an in situ nitrogen doping method combined with K_2CO_3 activation. The study systematically examined how changes in the physical structure and surface properties of the porous carbons affected their CH_4/N_2 separation performance. The results revealed that in situ nitrogen doping not only effectively adjusts the pore structure and alters the reaction of K_2CO_3 on the carbon matrix, but also introduces nitrogen and oxygen functional groups that significantly enhance the adsorption capabilities of the materials. In particular, sample S_3Y_6-800 demonstrated the highest methane adsorption capacity of 2.23 mmol/g at 273 K and 1 bar, outperforming most other porous carbons. This exceptional performance is attributed to the introduction of N-5, N-6, C-O, and COOH functional groups, as well as a narrower pore-size distribution (0.5–0.7 nm) and the formation of carbon nanotube structures. The introduction of heteroatoms also provides additional adsorption sites for the porous carbon, thus improving its methane adsorption capacity. Furthermore, dynamic breakthrough experiments confirmed that all samples effectively separated methane and nitrogen. The Toth model accurately described the CH_4 adsorption behavior on S_3Y_6-800 at 298 K, suggesting that the adsorption process follows a sub-monolayer coverage mechanism within the microporous regions. This study provides a mild and environmentally friendly preparation method of porous carbons for CH_4/N_2 separation.

Keywords: N-doped porous carbon; CH_4/N_2 separation; corn protein powder; K_2CO_3 activation; narrow micropores

check for updates

Academic Editor: Dimosthenis Giokas

Received: 30 December 2024
Revised: 30 January 2025
Accepted: 6 February 2025
Published: 8 February 2025

Citation: Wang, H.; Zhao, Y.; Lian, H.; Wang, Q.; Shang, Z.; Zhang, G. In Situ N-Doped Low-Corrosion Porous Carbon Derived from Biomass for Efficient CH_4/N_2 Separation. *Separations* **2025**, *12*, 42. https://doi.org/10.3390/separations12020042

Copyright: © 2025 by the authors. Licensee MDPI, Basel, Switzerland. This article is an open access article distributed under the terms and conditions of the Creative Commons Attribution (CC BY) license (https://creativecommons.org/licenses/by/4.0/).

1. Introduction

With the growing global demand for energy, natural gas is gaining increasing attention as a relatively clean and efficient energy source. Among unconventional energy resources, coalbed methane (CBM) holds significant multidimensional development potential [1]. Particularly in the context of rising global demand for clean energy, CBM, as a low-carbon and environmentally friendly energy option, demonstrates substantial potential for development. Its exploitation not only contributes to optimizing the energy mix but also enhances coal mine safety. The primary component of CBM is methane (CH_4), but it is typically accompanied by a large proportion of impurity gases, such as N_2, O_2, CO_2, and H_2O. These impurities not only reduce the calorific value of methane but also negatively affect the overall efficiency of CBM utilization [2]. Consequently, this low-quality natural

gas cannot be used directly as fuel and is often vented into the atmosphere, leading to resource wastage and environmental pollution. Therefore, enhancing the methane content of CBM and removing impurity gases, particularly nitrogen, have become key technical challenges for improving the efficiency of CBM utilization [3].

Among the various gas separation technologies, PSA has emerged as an effective technique for CBM separation due to its simplicity, low operating costs, and environmental friendliness [4]. The core of PSA technology lies in the development of efficient, low-cost, and renewable adsorbents. These adsorbents must not only possess a high specific surface area and adsorption capacity but also demonstrate excellent CH_4/N_2 selectivity, chemical stability, and regenerability [5]. Current adsorbents include zeolite molecular sieves [6], metal–organic frameworks (MOFs) [7], and porous carbon [8]. In particular, porous carbon has demonstrated unique advantages in CH_4/N_2 separation due to its widespread availability, low cost, tunable pore structure, and the ease with which its surface chemistry can be modified [9].

In the past few years, the research on porous carbon materials has focused on the preparation of high-performance carbon activated by chemical activation. Activators play a crucial role in this process. Commonly used activators include KOH, $ZnCl_2$, H_3PO_4, and K_2CO_3, each of which has unique characteristics suited for different applications and significantly influences the properties of the final product. KOH is a common choice for the preparation of high-specific-surface-area and microporous materials because it is able to effectively break the C-C bonds in the carbon skeleton at high temperatures and form a rich microporous structure. However, KOH is highly corrosive and may cause damage to equipment, and its use can cause pollution to the environment [10]. Zheng et al. studied the effect of activation temperature on methane adsorption performance using coal as the carbon source and KOH as the activator [11]. Similarly, Zhang et al. used corn cob as the raw material and created porous carbon with an adjustable pore size through KOH activation [12]. Although the effect of KOH activation is remarkable, its strong corrosiveness and environmental pollution should not be ignored. Phosphoric acid (H_3PO_4) activation is usually accomplished at lower temperatures and mainly produces mesoporous materials. Due to the acidic nature of phosphoric acid, it may inhibit the retention of nitrogen species. Andia et al. used H_3PO_4 to activate six different biomasses and produced wood-based porous carbons with a high specific surface area (1244.62 m^2/g) and large mesoporous volume (1.0549 cm^3/g) [13]. $ZnCl_2$ is a milder activator but does not promote the formation of many micropores and releases harmful by-products during activation. Bicil et al. prepared activated carbons with well-developed porous structures and high surface areas from almond shells using $ZnCl_2$, investigating the impact of activator dosage on the morphology of the carbon materials [14]. The selection of suitable activators is crucial to balance performance, cost, and environmental impact. In recent years, the research focus has shifted to the selection of an environmentally friendly and efficient green activator. Similar to KOH, K_2CO_3 can react with the carbon source to remove impurities and open the pore structure. K_2CO_3 has a lower activation temperature and a milder reaction, which is environmentally friendly, and thus shows a wider application in the preparation of carbon materials. However, the formation of pores during K_2CO_3 activation is significantly affected by the reaction temperature and reaction time, resulting in most porous carbon materials being dominated by mesopores and macropores, with a relatively low proportion of micropores [15].

To improve the efficiency of CH_4/N_2 separation, researchers have turned to heteroatom doping strategies. Nitrogen doping has been shown to effectively modulate the pore structure of porous carbon, particularly in promoting the formation of micropores, which in turn enhances the adsorption selectivity for CH_4/N_2 [16]. The self-doped nitrogen

technique is particularly favored due to its simplicity and the absence of costly chemical additives, ensuring a uniform distribution of nitrogen within the porous carbon [17]. Common nitrogen sources include organic nitrogen compounds, high-nitrogen biomass materials, and natural protein-based substances. Corn protein powder, as a natural nitrogen source, is widely available, renewable, and has a low environmental impact [18]. Compared to traditional chemical nitrogen sources (e.g., ammonia, urea), corn protein powder offers more environmentally friendly advantages in the nitrogen doping process. It is rich in amino acids and peptide chains, which, under high-temperature conditions, can effectively incorporate nitrogen into porous carbon to form a variety of nitrogen-based functional groups, such as pyridinic nitrogen and pyrrolic nitrogen [19]. Therefore, in situ nitrogen doping of corn protein powder mixed with carbon precursors such as pine wood chips not only realizes the effective utilization of agricultural waste, but also promotes the development of a circular economy. By converting the waste into high-value-added activated carbon materials, the waste of resources is reduced and the process of sustainable development is promoted. Li et al. prepared porous carbon using discarded wool as the carbon source, urea as the nitrogen source, and KOH as the activator, and the adsorption capacity of the prepared porous carbon was 1.01 mmol/g at 298 K, 1 atm [20].

In this study, a range of high-performance nitrogen-doped porous carbons were synthesized by in situ nitrogen doping of pine sawdust using corn protein powder, followed by K_2CO_3 activation. The study thoroughly examines the impact of nitrogen doping and activation temperature on the porous carbon structure. Particular focus is given to understanding the correlation between the structure and surface characteristics of the porous carbons and their ability to separate CH_4 from N_2. The kinetics and efficiency of the adsorbents are further evaluated through fixed-bed permeation experiments and adsorption thermodynamics. The environmentally friendly and mild preparation method introduced in this study offers a novel approach to producing porous carbon materials. This approach not only facilitates waste reuse but also enhances material performance, offering a more competitive technological solution for CH_4 and N_2 separation in coalbed methane. This innovative technique addresses the economic challenges of conventional methods while prioritizing environmental sustainability, highlighting its promising potential for widespread application.

2. Materials and Methods

2.1. Materials

Pine chips and corn protein powder were obtained from Surui Agricultural Products Deep Processing Plant, Jiangsu Province, China, and the results of the elemental analysis are presented in Table 1. Surface contaminants were removed by washing with deionized water, followed by drying in an oven at 110 °C overnight, after which they were stored in a sealed bag for future use. K_2CO_3 (99.99%) was supplied by Aladdin Biochemical Technology Co., Ltd. in Shanghai, China, and CH_4 (99.999%) and N_2 (99.999%) were supplied by Taiyuan Taineng Gas Co. in Taiyuan, China.

Table 1. Elemental analysis of pine wood chips and maize protein powder.

Sample	Ultimate Analysis (wt.%), daf				
	C	H	O [a]	N	S
Pine chips	52.21	6.09	41.41	0.29	0
Corn protein powder	49.04	6.90	31.19	12.23	0.64
S_3Y_6-800	87.58	0.89	9.30	2.23	0

[a] Calculated by difference.

2.2. Preparation of Nitrogen-Doped Porous Carbon

For the preparation of porous carbon, we used a two-step method to prepare porous carbon. The first step was the charring stage: 5 g of pine (S), 5 g of corn protein powder (Y), 3 g of pine powder and 6 g of corn protein powder, 5 g of pine powder and 5 g of corn protein powder, 6 g of pine powder and 3 g of corn protein powder, respectively, were taken in a mortar and grinded thoroughly in order to be mixed homogeneously, and then the homogeneously mixed samples were heated in a tube furnace under N_2 atmosphere at a heating rate of 10 °C/min to 500 °C after a constant temperature of 2 h. The carbonized samples were "S, Y, S_3Y_6, S_5Y_5, S_6Y_3".

The second step was the activation stage: 3-fold loading of K_2CO_3 on SY was placed in a closed reaction tank using the milling method. The closed reaction jar containing the sample was placed in a muffle furnace and activated at the same rate of heating up to a certain temperature for 90 min. After activation, the sample was washed with deionized water until the filtrate pH = 7 or so. The activated sample is noted as "S_xY_z-". x and z are the amounts of pine chips and corn protein powder, respectively. For example, S_3Y_6-800 is the porous carbon obtained by heating pine wood with corn protein powder of mass 3 g and 6 g to 800 °C after the above steps.

The yield of porous carbon was calculated according to the Equation (1):

$$Y = \frac{m_2}{m_1} \tag{1}$$

where m_2 represents the mass of the porous carbon and m_1 is the mass of the carbon source; the data obtained for the yield are shown in Table S1.

2.3. Characterization

Porous carbon was analyzed using SEM, XRD, BET, FTIR, and XPS; see the Supporting Information for the characterization process.

2.4. Adsorption Performance

In this research, the nitrogen and methane adsorption isotherms were measured at 298 K and 273 K using a BSD-PS2 Gas Adsorption Analyzer (Best Instrument Technology Co., Ltd., Beijing, China) and a MicroActive ASAP 2460 Gas Adsorption Analyzer(McMurray Tick Instruments Co., Ltd., Shanghai, China), respectively. The Ideal Adsorption Solution Theory (IAST) was employed to predict the CH_4/N_2 selectivity. To obtain the necessary data for IAST, the CH_4/N_2 adsorption isotherm was fitted using the Langmuir isothermal adsorption model [21]. The CH_4/N_2 selectivity was then calculated using Equation (2).

$$S_{ads} = \frac{X_1/X_2}{Y_1/Y_2} \tag{2}$$

where S_{ads} is the adsorption selectivity, and X_i and Y_i denote the molar fraction of component i in the adsorption phase and the molar fraction of component i in the gas phase of component i (i = 1, 2), respectively.

The equivalent heat of adsorption of CH_4 and N_2 was calculated from the adsorption isotherm by the Clausis–Clapeyron equation [22]. The Clausis–Clapeyron equation is given below:

$$\ln(\frac{P_1}{P_2}) = -\frac{\Delta H_{ads}}{R}(\frac{1}{T_2} - \frac{1}{T_1}) \tag{3}$$

where ΔH_{ads} denotes the strength of interaction between gas molecules and the adsorbent (kJ/mol); R is the universal gas constant with a value of 8.314 J/mol^{-1}K^{-1}. T_1 and T_2 are 298 K and 273 K, respectively, whereas P_1 and P_2 are adsorption pressures for the same

adsorption amount at 298 K and 273 K. The adsorption pressure was calculated by using the following formula.

2.5. Breakthrough Experiment of CH_4 and N_2 Binary Mixture Gas

The breakthrough experiments were conducted using a custom-designed dynamic permeation profiling apparatus. The experimental setup and schematic representation of the apparatus can be found in Figure S1. The main steps of the procedure are as follows. First, the adsorbent samples were first dried in an oven at 80 °C to remove any residual moisture. The dried sample was then sieved to a particle size of <149 μm to ensure homogeneity. The gas mixture of CH_4 and N_2 was introduced into the system at a 1:1 ratio using a mass flow controller, with the total flow rate set to 10 mL/min. Prior to the introduction of the gas mixtures, the adsorbent bed was cleaned using a helium flow rate (35 mL/min) for 15 min to remove any contaminants or impurities that may have been present. Subsequently, 1 g of adsorbent sample was carefully loaded into an adsorbent column with an inner diameter of 9 mm. To ensure the removal of any residual gases from the separation column, the gas source was switched to helium, and the system was flushed until it was fully purged with helium. Afterward, the valve connecting the adsorption system to the external system was closed, and the system was evacuated to a pressure of −0.1 MPa. This process was repeated multiple times, alternating between helium flushing and evacuation, to ensure complete removal of all residual gases. After completing the pretreatment, the gas source was switched to methane and nitrogen. Gas samples were collected at 20 s intervals until the adsorbent bed reached saturation. The collected gas samples were analyzed using a gas chromatograph to accurately determine the concentrations of CH_4 and N_2. The resulting data were then used to construct permeation curves, representing the concentration of each gas as a function of time.

3. Results and Discussion

3.1. Pore Structure and Surface Morphology of Porous Carbon

The N_2 adsorption–desorption isotherms and pore size distributions of all samples are shown in Figure 1a. Based on the IUPAC classification, all samples exhibited type I isotherm characteristics. At low pressure ($P/P_0 < 0.1$), the N_2 adsorption increased sharply and reached a saturation plateau, indicating the presence of microporous structures. This rapid adsorption suggests a strong interaction between the N_2 molecules and the microporous surfaces, leading to the quick filling of the micropores. As the P/P_0 value increased, the adsorption stabilized, indicating that the micropores were nearly filled and no significant further adsorption occurred. When $P/P_0 > 0.45$, hysteresis loops appeared in the isotherms, suggesting that all the samples contained varying degrees of mesoporous structures.

The pore structure parameters for all samples are summarized in Table 2. The specific surface area and pore volume of the pure pine wood chips carbon material were 562 m^2/g and 0.31 cm^3/g, respectively. In contrast, both the specific surface area, pore volume, and the proportion of micropores significantly increased as the doping ratio of corn protein powder rose. This suggests that the addition of corn protein powder reduces the interaction between K_2CO_3 and the carbon substrate, resulting in the formation of more micropores. This effect is linked to the superior decomposition capacity of corn protein powder, and as the doping ratio increases, the decomposition of the mixture at high temperatures (800 °C) also intensifies, promoting the carbonization process and thereby increasing the specific surface area and pore volume [23].

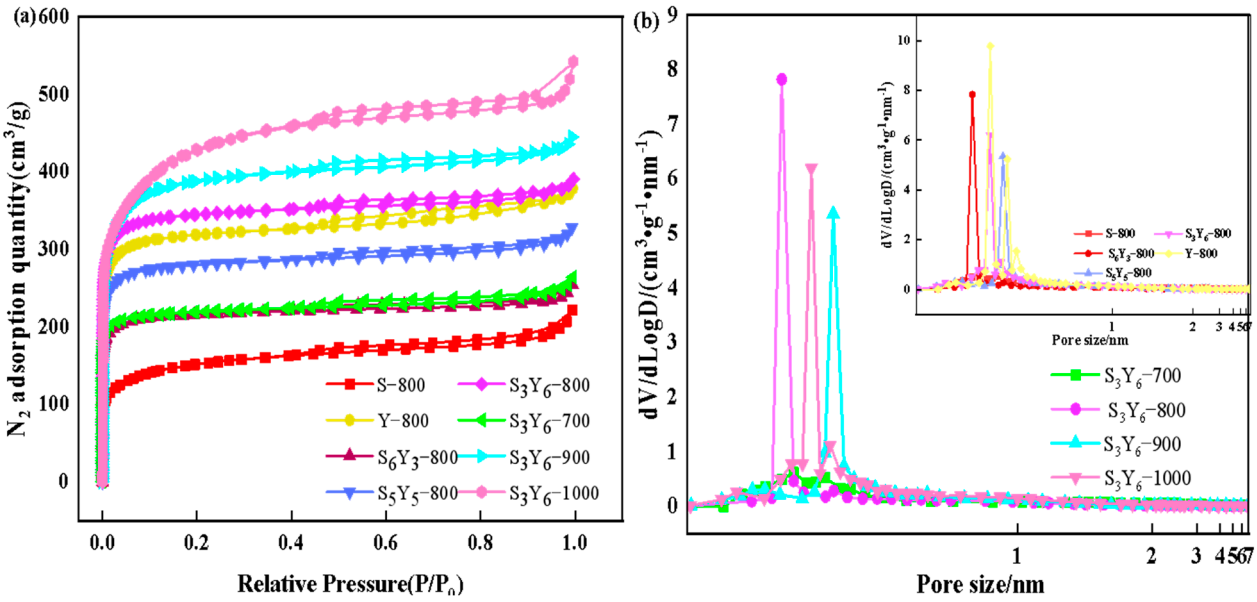


Figure 1. For all samples: (**a**) N_2 adsorption–desorption curves; (**b**) pore size distribution by NLDFT method.

Table 2. Pore structure parameters of the samples.

Sample	Specific Surface Area ($m^2 \cdot g^{-1}$)	Pore Volume ($cm^3 \cdot g^{-1}$)	Micropore Volume ($cm^3 \cdot g^{-1}$)	Average Pore Diameter (nm)	V_m/V_t (%)
S−800	562	0.31	0.23	2.38	74
Y−800	1267	0.57	0.45	1.82	78
S_6Y_3−800	864	0.37	0.33	1.78	89
S_5Y_5−800	1115	0.49	0.43	1.8	91
S_3Y_6−800	1377	0.59	0.53	1.73	90
S_3Y_6−700	878	0.39	0.34	1.83	87
S_3Y_6−900	1500	0.67	0.60	1.82	90
S_3Y_6−1000	1575	0.80	0.65	2.05	81

When the doping ratio of corn protein powder was held constant at S_3Y_6, both the specific surface area and pore volume showed a marked increase as the activation temperature rose from 700 °C to 1000 °C, with the specific surface area increasing from 878 m^2/g to 1575 m^2/g, and the pore volume rising from 0.39 cm^3/g to 0.80 cm^3/g. The higher activation temperature enhanced the reaction between K_2CO_3 and the carbon matrix, promoting the formation of additional pore channels, which further improved both microporous and mesoporous structures and increased the specific surface area and pore volume. However, it is noteworthy that when the activation temperature increased from 900 °C to 1000 °C, the proportion of micropores decreased from 90% to 81%, even though the total pore volume and microporous volume still showed an increasing trend. This phenomenon can be attributed to the increase in mesopores caused by excessively high temperatures, which allowed for a more complete reaction between K_2CO_3 and the carbon matrix. As a result, some of the micropores were transformed into mesopores or macropores. In addition, Figure 1b illustrates that micropores smaller than 1 nm in all samples were mainly concentrated in the 0.5–0.7 nm range. As the doping ratio of corn protein powder increased, the volume of micropores in the 0.5–0.7 nm range expanded significantly. When the doping ratio was fixed at S_3Y_6 and the temperature was increased from 700 °C to 800 °C, the volume of micropores in the 0.5–0.7 nm range also increased obviously. However, when the temperature was further raised to 900 °C or 1000 °C, the volume of ultramicropores in

the range of 0.5–0.7 nm remained unchanged or slightly decreased, while the increase in microporous volume was more concentrated in the 0.7–2 nm range. According to a related study [24], micropores within V < 0.8 nm were particularly favorable for the adsorption of CH_4 molecules and had a significant effect on the selective adsorption of CH_4/N_2.

To further analyze the surface morphology of the samples, all samples were examined using scanning electron microscopy (SEM). As shown in Figure 2a, the surface of the K_2CO_3-activated S−800 samples exhibited an aggregated, rough granular morphology. This phenomenon can be attributed to the strong etching interaction between K_2CO_3 and the pine shavings at a high activation temperature of 800 °C. Figure 2b presents the surface morphology of the Y−800 sample, which displays a distinct spongy structure with a looser, more porous surface and a denser pore distribution. These observations are consistent with the results from the N_2 adsorption–desorption experiments. Figure 2c illustrates the surface morphology of the S_6Y_3−800 sample. In comparison to S_3Y_6−800, the pore structure of S_6Y_3−800 was significantly reduced, with an increase in rod-like structures and a decrease in sponge-like structures. This suggests that variations in the doping ratio of corn protein powder have a marked impact on the surface morphology of the porous carbon, which in turn influences its pore structure and overall properties. The surface morphology of the samples shows a certain regularity as the temperature changes. When the activation temperature was 700 °C (Figure 2f), the surface of the S_3Y_6−700 sample exhibited large, irregular massive particles. This can be attributed to the weak K_2CO_3 activation at lower temperatures, which fails to fully react with the carbon matrix, resulting in incomplete formation of pore structures. However, when the temperature was increased to 800 °C, the surface of the S_3Y_6−800 sample displayed a dense spongy structure, accompanied by a significant increase in the pore structure. It is worth noting that the appearance of some of the rod-like structures is related to the generation of carbon nanotubes, which not only enhance the mechanical support of the carbon material and reduce the structural loss caused by the pore overlap, but also construct a three-dimensional (3D) network, which improves the gas molecule transport efficiency, and consequently the adsorption performance [25]. When the activation temperature was further raised to 900 °C, the surface characteristics of the S_3Y_6−900 sample changed significantly. The spongy structure originally present almost disappeared and was replaced by aggregated spherical particles, while more carbon nanotube generation was observed. This phenomenon can be attributed to the fact that a large number of volatile components were released under high-temperature conditions at 900 °C, leading to a shift in the surface morphology of the material. Previous studies have shown that K ions play a very important role in this process. Specifically, K ions not only promoted the release of carbon-containing gases and aromatic compounds during biomass pyrolysis, but also accelerated the polymerization reaction of these gases, which ultimately promoted the formation of carbon nanotubes [26,27]. Therefore, K_2CO_3 plays a dual role in the activation process of carbon: on the one hand, it acts as an activator to promote the generation of pore structures by undergoing an etching reaction with the carbon matrix; on the other hand, it acts as a catalyst to promote the growth of carbon nanotubes by catalyzing the release of carbon sources. This dual function makes K_2CO_3 play an important role in regulating the microstructure of carbon materials, which affects their adsorption properties and other physicochemical properties. The transformation of micropores into mesopores and macropores as the temperature increases to 1000 °C suggests that excessively high activation temperatures promote the thorough reaction of K_2CO_3 with the carbon substrate, causing some micropores to merge into mesopores and macropores. Given the excellent pore structure observed in the S_3Y_6−800 sample, subsequent studies will focus on examining the effects of temperature on the properties of porous carbon at this specific doping ratio.

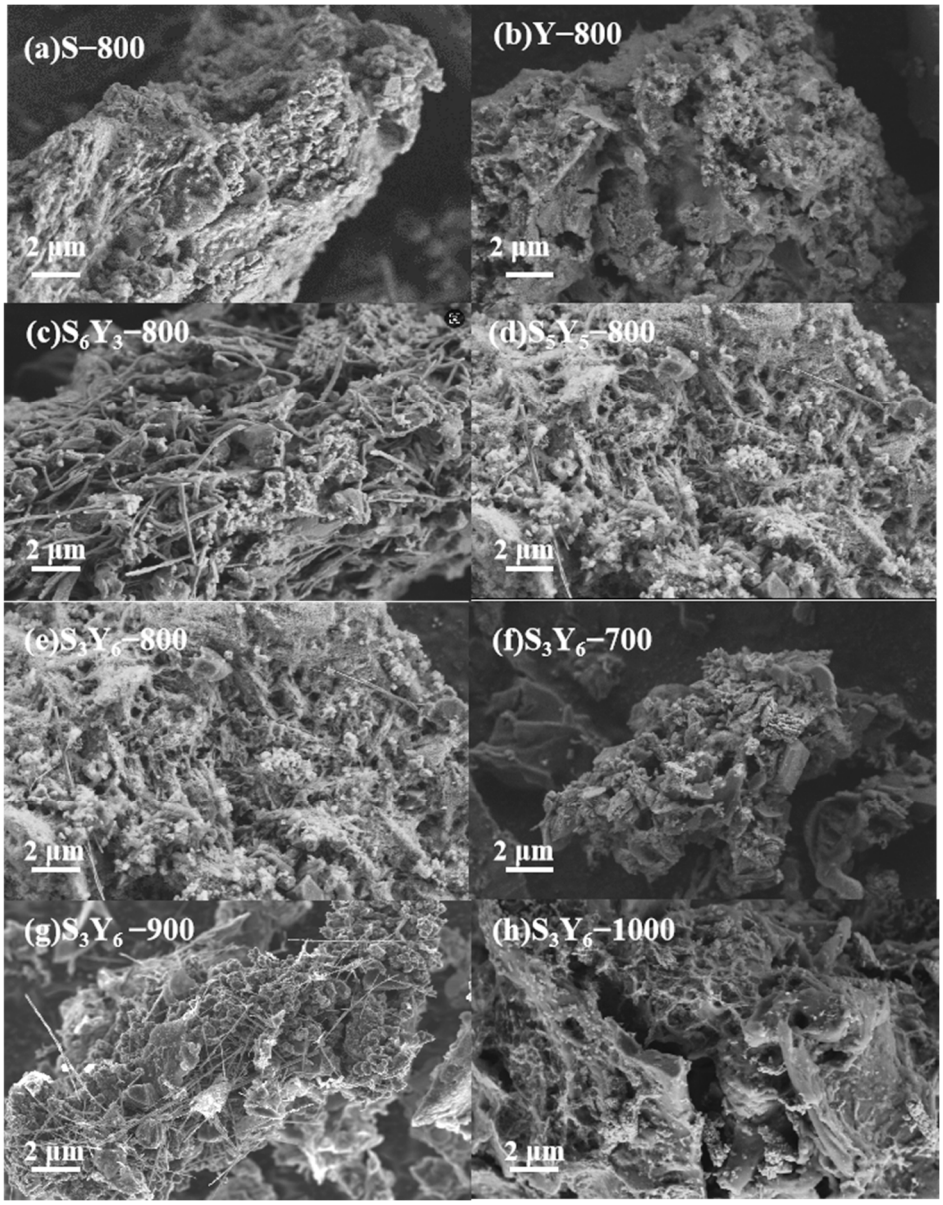


Figure 2. SEM images of all samples.

3.2. Crystallinity of Porous Carbon and Changes in Surface Functional Groups

Figure 3a displays the X-ray diffraction (XRD) patterns of all the samples. The findings show two prominent diffraction peaks at 23° and 43°, corresponding to the (002) and (101) planes of graphite, respectively [28]. As the activation temperature increases from 700 °C to 800 °C, the intensity of these diffraction peaks decreases, indicating that the porous carbon becomes more disordered and predominantly exists as amorphous carbon. The decrease in crystallinity is due to the enhanced activation reaction between K_2CO_3 and the carbon substrate at high temperatures, leading to a more disordered structure. However, when the activation temperature was further increased to 900 °C, the (002) diffraction peak became sharper, suggesting a significant improvement in the ordering of the carbon structure. This change is related to the generation of CNTs, since the formation of CNTs enhances the crystallinity of the carbon material to some extent. In addition, the vigorous reaction under high-temperature conditions may lead to the generation of more CNTs, which further enhances the crystallinity and structural ordering of the materials [29].

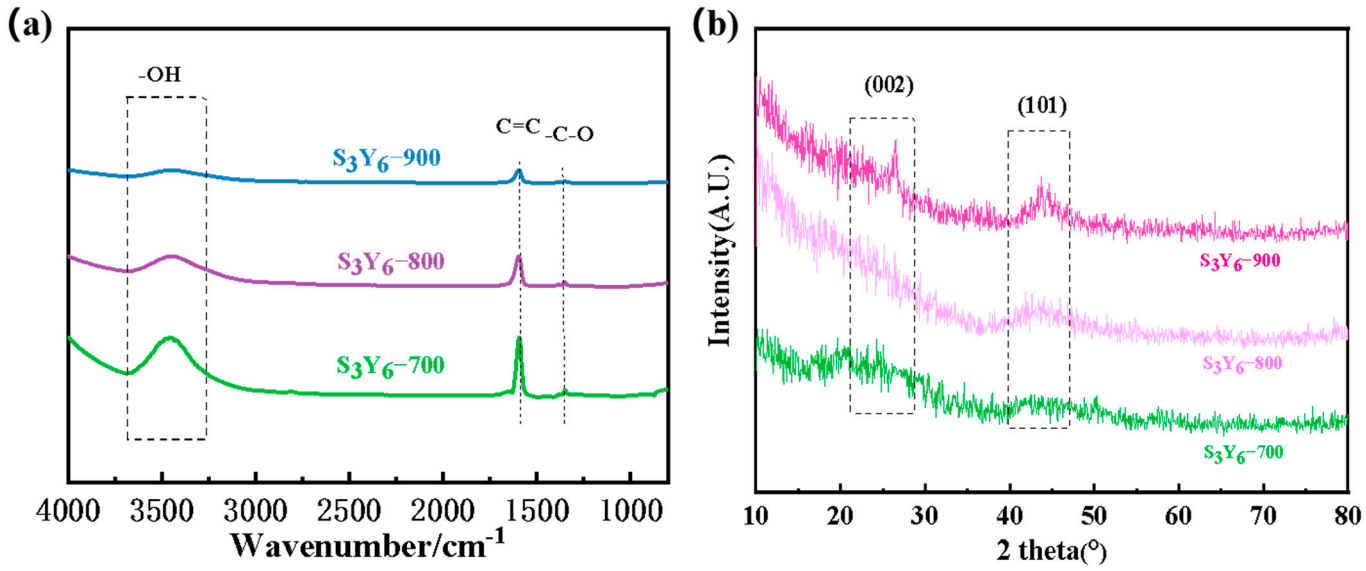


Figure 3. (**a**) XRD diagrams of samples S_3Y_6-700, S_3Y_6-800, and S_3Y_6-900; (**b**) FT-IR of samples S_3Y_6-700, S_3Y_6-800, and S_3Y_6-900.

Figure 3b presents the Fourier transform infrared (FT-IR) spectra of sample S_3Y_6 at different activation temperatures, reflecting changes in the surface functional groups. Among them, the broad peak at 3443 cm^{-1} is an O-H stretching vibration peak, and the peak near 1591 cm^{-1} may be attributed to C=O stretching vibration. The intensity of the peak at 1349 cm^{-1} is lower and can be attributed to the attributed -C-O [30]. The obvious weakening of the -OH diffraction peak with increasing activation temperature suggests that the activation reaction becomes more intense with increasing temperature, which promotes the graphitization process and leads to the release of oxygen atoms [31]. It is also noteworthy that the strength of the C=C bond decreases significantly at high temperatures. This suggests that the aromatic ring structure (C=C) in carbon materials undergoes decomposition and transformation at high temperatures, further demonstrating the complex chemical changes during the activation process. As the temperature increases, these aromatic ring structures are gradually destroyed and transformed into more stable graphitized structures.

3.3. Surface Chemistry of Porous Carbon

To further investigate the surface composition and chemical properties of the samples, X-ray photoelectron spectroscopy (XPS) was utilized to analyze the samples at different activation temperatures in detail. As shown in Table 1, the carbon content of S_3Y_6-800 was higher than that of S, indicating that the addition of corn protein powder promoted the degree of carbonization of pine wood. Figure 4a–c presents the high-resolution N1s spectra of sample S_3Y_6 at 700 °C, 800 °C, and 900 °C. The deconvolution analysis of the N1s spectral peaks revealed four major peaks at 398.5 ± 0.1 eV, 399.7 ± 0.1 eV, 400.2 ± 0.1 eV, and 401.4 ± 0.1 eV. These peaks correspond to pyridinic nitrogen (N-6), amine nitrogen (N), pyrrolic nitrogen (N-5)/pyridinic nitrogen (N-6), and graphitic nitrogen (N-Q), respectively [32]. Although XPS is not yet capable of precisely distinguishing between N-5 and N-6 types of nitrogen, previous studies have indicated that N-5 is more stable than N-6 under high-temperature conditions [33]. Therefore, the peak at 400.2 ± 0.1 eV is classified as pyrrolic nitrogen (N-5). As can be seen in Table 3, the nitrogen content in all samples is generally low, a phenomenon that stems from the significant loss of nitrogen during high-temperature activation [34]. As the activation temperature increased from 700 °C to 900 °C, the total content of pyrrole nitrogen (N-5) and pyridine nitrogen (N-6) decreased

significantly from 56% to 37.38%, whereas the content of graphite nitrogen (N-Q) increased from 16.11% to 31.45%. This shift suggests that the N-5 and N-6 groups are gradually transformed into the more stable N-Q form at higher temperatures. This transformation not only reflects changes in the material's internal structure but also influences its surface chemistry. Notably, the higher contents of pyrrole nitrogen (N-5) and pyridine nitrogen (N-6) not only increase the basicity of the microporous carbon surface but also generate numerous active sites on the material's surface. These nitrogen functional groups enhance surface polarization and promote interactions with CH_4 molecules by increasing surface polarity and electron density. Specifically, the presence of pyrrole nitrogen and pyridine nitrogen makes the material's surface more reactive, effectively trapping and immobilizing gas molecules, thereby improving adsorption properties. Moreover, these nitrogen groups can act as anchor sites, providing additional binding sites that facilitate the efficient adsorption and separation of small molecule gases [8,35].

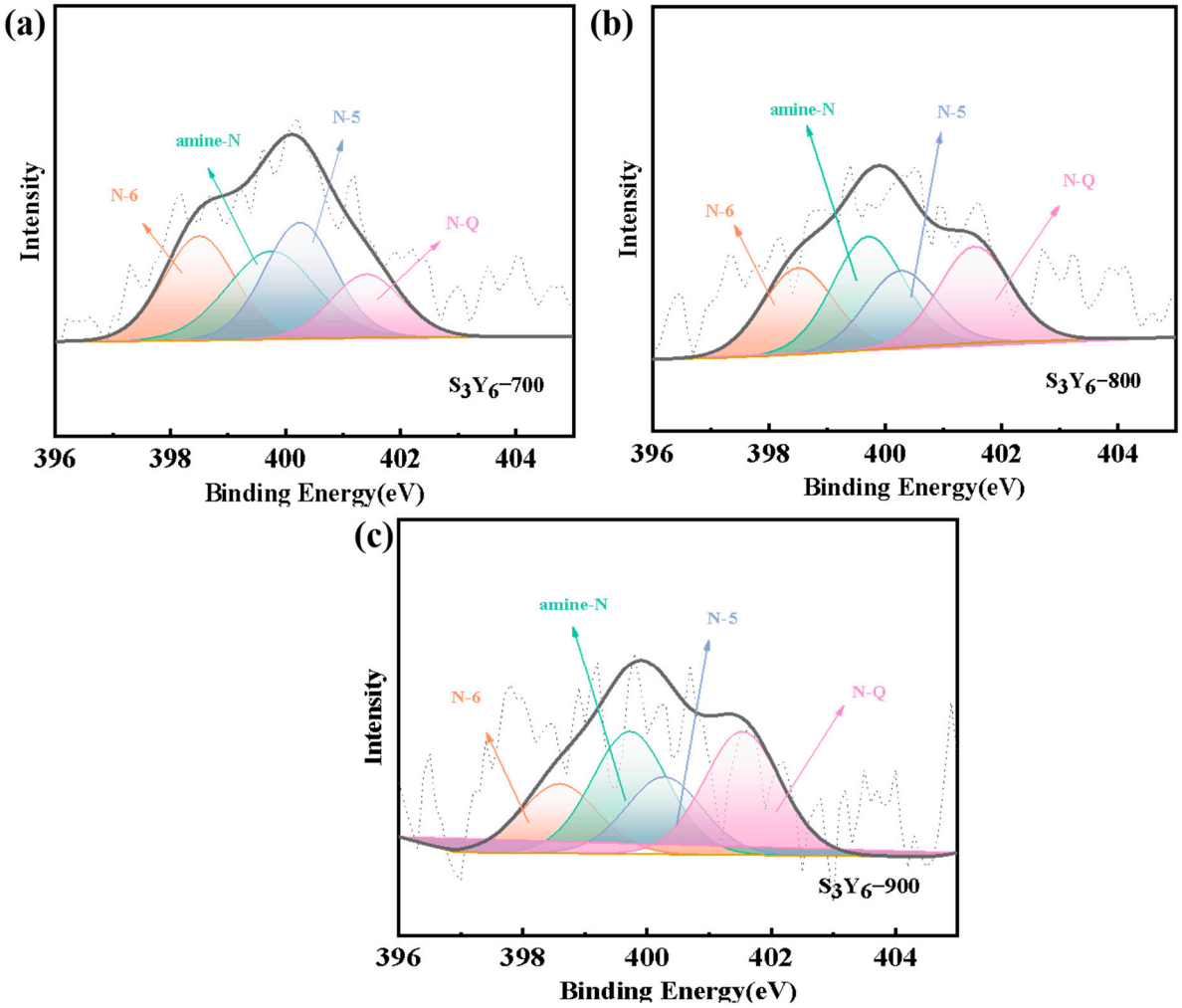


Figure 4. N1s spectra of (**a**) S_3Y_6-700; (**b**) S_3Y_6-800; and (**c**) S_3Y_6-900.

To further investigate the characteristics of the oxygen-containing functional groups in the samples, the O1s spectra were analyzed and fitted. The results are shown in Figure 5. The fitting analysis revealed four distinct peaks at 531.1–531.4 eV, 532.3–532.8 eV, 533.1–533.5 eV, and 534.5–535.3 eV, which correspond to C=O (O1), C=O (O2), C-O (O3), and COOH (O4) [36], respectively. As observed in the figure, the samples contain a significant proportion of C=O, C-O, COOH, and oxygen-containing functional groups that are adsorbed from surface moisture or oxygen. Tables 4 and 5 demonstrate the content

and concentration of different oxygen species in the O1s spectra. According to the data in Table 5, the total content of oxygen-containing functional groups in the S_3Y_6 samples decreased from 22.02% to 16.55% as the temperature increased from 700 °C to 900 °C. This decrease is mainly attributed to the reduction of C=O groups, which are unstable at high temperatures and prone to decomposition or conversion into other functional groups [37]. In contrast, the proportion of C-O functional groups increased, due to the enhanced formation of C-O-like groups under high-temperature conditions. Notably, a certain amount of C-O and OH groups in the samples can significantly increase the polarity of the material surface and provide more active sites, which can help the capture and immobilization of gas molecules, and thus can promote the adsorption of CH_4 molecules [31]. Therefore, while the high-temperature activation process leads to a reduction in some oxygen-containing functional groups, the increase in C-O and OH groups still contributes positively to the optimization of the gas adsorption properties of the materials.

Table 3. Nitrogen components in N1s spectra.

Sample	N/at. %	N Species Ratio [A]				N Species Ratio [B]			
		N-6/%	Amine-N	N-5/%	N-Q	N-6/%	Amine-N	N-5/%	N-Q
S_3Y_6−700	2.37	26.55	27.89	29.45	16.11	0.63	0.66	0.70	0.38
S_3Y_6−800	1.77	23.30	30.49	20.27	25.94	0.41	0.54	0.36	0.46
S_3Y_6−900	1.07	17.66	31.17	19.72	31.45	0.19	0.33	0.21	0.34

[A] Percentage of each deconvoluted peak in relation to N1s total area (%). [B] Group concentration (wt.%). Concentration of different groups is calculated by multiplying percentage of deconvoluted peak by nitrogen concentration. Thus, in case of S_3Y_6−700, percentage of N-6 (26.55%) multiplying oxygen content (2.37 wt.%) gives 0.63 wt.%.

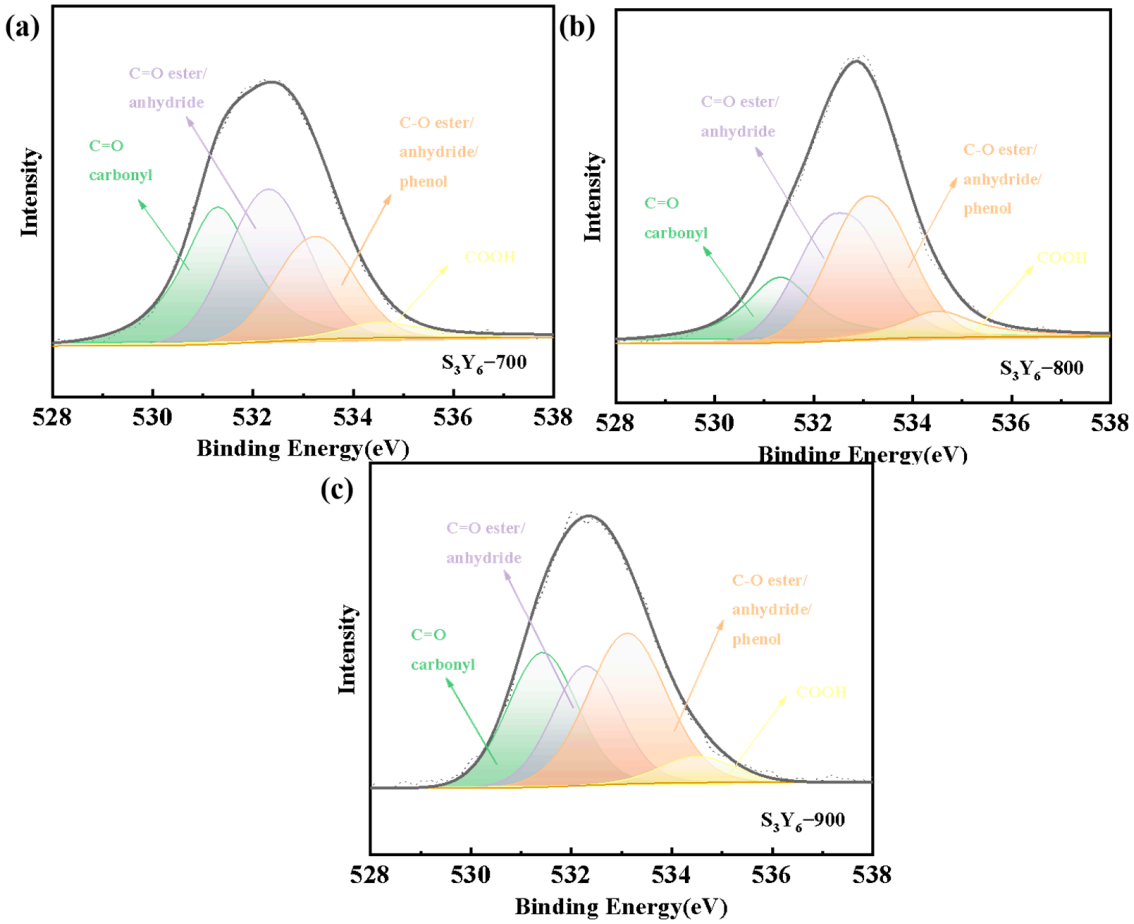


Figure 5. O1s spectra of (**a**) S_3Y_6−700; (**b**) S_3Y_6−800; and (**c**) S_3Y_6−900.

Table 4. Concentration of oxygen components in O1s spectra [A].

Sample	O Species Ratio [A]			
	O1/%	O2/%	O3/%	O4/%
S_3Y_6-700	33.63	36.02	23.95	6.41
S_3Y_6-800	20.06	33.99	36.43	9.52
S_3Y_6-900	30.09	25.71	38.06	6.14

[A] The percentage of each deconvoluted peak in relation to O1s total area (%).

Table 5. Concentration of oxygen components in O1s spectra [B].

Sample	O/at. %	O Species Ratio [B]			
		O1/%	O2/%	O3/%	O4/%
S_3Y_6-700	22.02	7.41	7.93	5.27	1.41
S_3Y_6-800	17.77	3.56	6.04	6.47	1.69
S_3Y_6-900	16.55	4.98	4.26	6.30	1.02

[B] Group concentration (wt.%). The concentration of different groups is calculated by multiplying the percentage of deconvoluted peak by oxygen concentration. Thus, in the case of S_3Y_6-700, the percentage of O1 (33.63%) multiplying the oxygen content (22.02 wt.%) gives 7.41 wt.%.

3.4. Adsorption and Separation of CH_4/N_2 by Porous Carbon

3.4.1. Pure Gas Adsorption Isotherm

To investigate the adsorption properties of N-doped porous carbon prepared at different activation temperatures for CH_4 and N_2, adsorption isotherms were measured at 273 K and 298 K. The results are presented in Figure 6 with detailed data in Table 6. The findings reveal that CH_4 adsorption is significantly higher at 273 K compared to 298 K, indicating that CH_4 adsorption is an exothermic physisorption process [38]. Furthermore, the adsorption capacity for CH_4 was generally greater than for N_2 at specific temperatures, primarily due to the higher polarizability of CH_4 compared to N_2. The increased polarizability of CH_4 enhances its interaction with the adsorbent surface, allowing more gas molecules to be adsorbed into the micropores. In contrast, N_2's lower polarizability weakens its interaction with the adsorbent, resulting in lower adsorption capacity [39]. Notably, S_3Y_6-800 exhibits the best CH_4 adsorption performance, despite having a smaller specific surface area and pore volume than S_3Y_6-900. At 273 K and 1 bar, the CH_4 adsorption of S_3Y_6-800 reached 2.23 mmol/g, compared to 1.47 mmol/g at 298 K and 1 bar. According to the literature, when the specific surface area of activated carbon exceeds 1000 m^2/g, the surface area is no longer the sole determinant of adsorption capacity, as the microporous structure and surface functional groups also play a crucial role in enhancing CH_4 adsorption. The nitrogen-doped porous carbon prepared here exhibits excellent CH_4 adsorption properties at low temperatures and high pressures, making it valuable for natural gas storage and transport.

To further explore the relationship between pore structure, surface properties, and CH_4 adsorption capacity, the microporous volume (V < 0.6 nm), along with specific N and O functional groups, were linearly correlated with the CH_4 adsorption capacity. The results of the fitting are shown in Figure 7. The data in the figure show that the correlation between microporous volume of V < 0.6 nm and CH_4 adsorption was low (R^2 = 0.43) at 298 K and 1 bar. In contrast, the specific N and O functional groups (N5 + N6 + O3 + O4) exhibited a much stronger linear relationship with CH_4 adsorption capacity, with R^2 values of 0.58 at 298 K and 0.86 at 1 bar. These results suggest that the N5 + N6 + O3 + O4 functional groups have a significant effect, while the microporous volume of V < 0.6 nm contributed relatively little to the adsorption capacity. This is due to the fact that the introduction of nitrogen-containing functional groups (e.g., N-5 and N-6) can significantly increase the

surface alkalinity and polarity of the carbon materials, thereby enhancing their electrostatic interactions with CH_4 molecules. Specifically, the N-5 and N-6 functional groups not only promote the surface polarization and dipole interactions of CH_4 molecules, but also increase the reactivity of the material surface to trap and immobilize gas molecules, further enhancing the adsorption efficiency [6]. On the other hand, C-O and COOH functional groups likewise positively affect the CH_4 adsorption capacity. For the pore volume aspect, the narrow microporous structure with V < 0.6 nm provides more accommodating space and the potential overlap between the pore walls enhances the interactions between the pore structures, both of which are favorable for CH_4 capture [40].

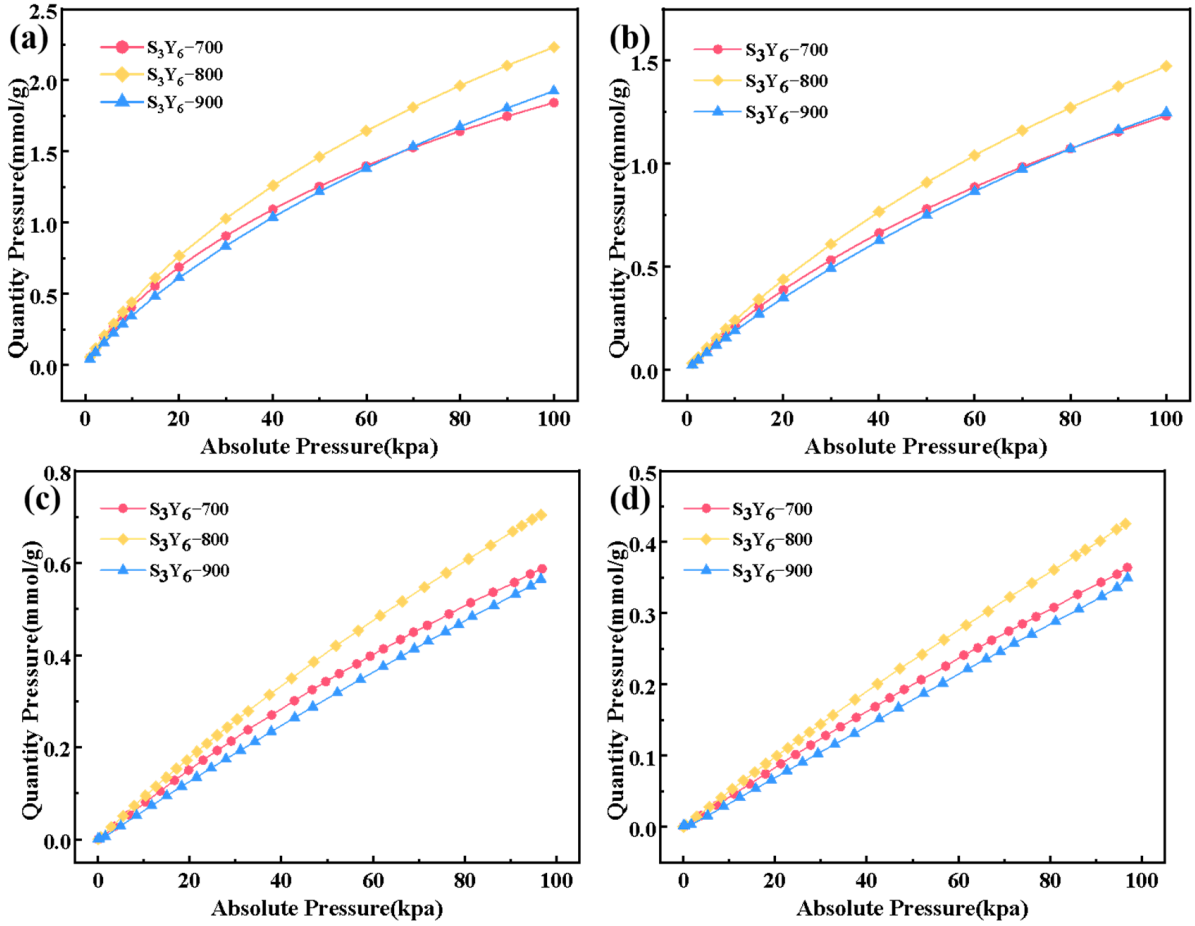


Figure 6. Adsorption isotherms of CH_4 for samples at (**a**) 273 K and (**b**) 298 K; adsorption isotherms of N_2 for samples at (**c**) 273 K and (**d**) 298 K.

Table 6. Adsorption of CH_4 and N_2 under different conditions.

Sample	273 K		298 K	
	CH_4 (mmol/g)	N_2 (mmol/g)	CH_4 (mmol/g)	N_2 (mmol/g)
S_3Y_6-700	1.84	0.59	1.23	0.36
S_3Y_6-800	2.23	0.70	1.47	0.43
S_3Y_6-900	1.93	0.56	1.24	0.35

3.4.2. Heat of Adsorption and Selectivity

In industrial applications, the adsorption performance of an adsorbent depends not only on its adsorption capacity for a target gas (e.g., CH_4) but also on its selectivity in gas mixtures (e.g., CH_4/N_2). To evaluate the adsorbent performance, the ISAT selectivity of the samples was calculated under CH_4/N_2 (20/80) and CH_4/N_2 (50/50) mixtures,

in addition to the determination of the adsorbed amount of CH_4 by the samples [41]. Figure 8a shows the CH_4/N_2 selectivities of S_3Y_6-700, S_3Y_6-800, and S_3Y_6-900 at 298 K, as calculated from the ideal adsorption solution. According to the literature, the CH_4/N_2 adsorption selectivity of commercial carbonaceous adsorbents typically ranges from 2.1 to 5.5 [42]. The selectivities of the prepared adsorbents for CH_4/N_2 were between 3.5 and 5 for both mixtures, in line with the requirements for commercial carbonaceous adsorbents. S_3Y_6-700 exhibited the highest adsorption selectivity, reaching 4.99 for CH_4/N_2 (20/80). This result suggests that, although the microporous volume of the samples follows the order $S_3Y_6-900 > S_3Y_6-800 > S_3Y_6-700$, the high selectivity of S_3Y_6-700 is attributed to the higher content of nitrogen-oxygen functional groups on its surface, which provide more active sites for CH_4 molecules and thus improve selectivity. The prepared adsorbents demonstrated superior separation performance under CH_4/N_2 (20/80) conditions. Figure 8c compares the performance of S_3Y_6-800 with other reported adsorbents in the CH_4/N_2 separation process at 298 K and 100 kPa. The results show that S_3Y_6-800 exhibits an excellent CH_4 adsorption capacity and its performance is competitive with existing adsorbents.

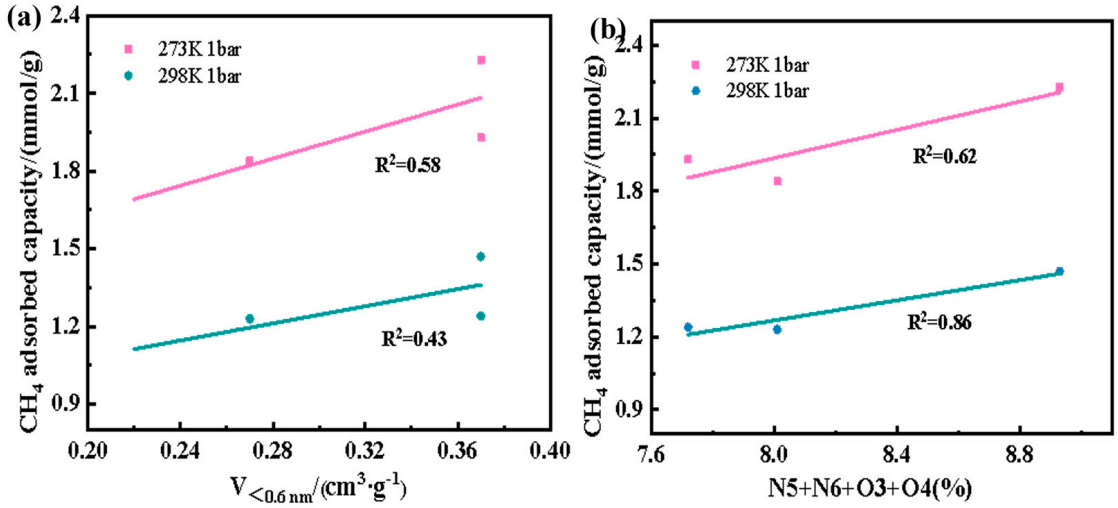


Figure 7. Correlation between (**a**) V < 0.6 nm; (**b**) N5 + N6 + O3 + O4.

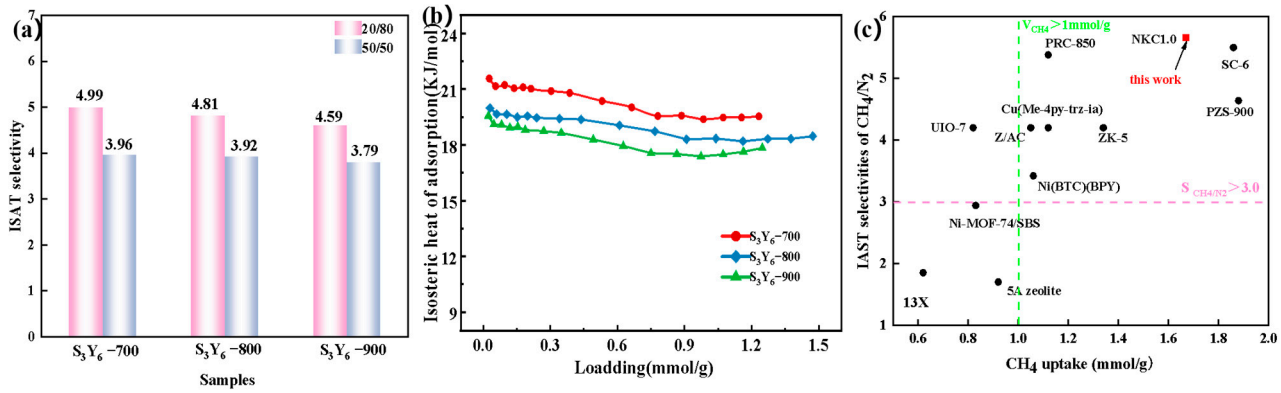


Figure 8. (**a**) Selectivity of all samples; (**b**) isosteric heats of adsorption; (**c**) comparison of CH_4/N_2 selectivity and CH_4 adsorption capacity.

A good adsorbent should also have excellent regeneration properties in addition to high adsorption capacity and selectivity. The heat of adsorption is a key factor for the adsorption and desorption processes of CH_4. A lower heat of adsorption helps to achieve efficient adsorption and desorption processes under mild conditions, thus reducing op-

erational energy consumption and preventing material damage due to high-temperature desorption as well. To further explore this property, the isotropic heat of adsorption (Q_{st}) of the sample was calculated using the Clausius–Clapeyron equation [43], and the results are shown in Figure 8b. The magnitude of the heat of adsorption is in the order of $S_3Y_6-700 > S_3Y_6-800 > S_3Y_6-900$ and diminishes with the increase in activation temperature. This indicates a typical physical exothermic process between CH_4 and the adsorbent. In addition, the heat of adsorption shows a downward trend as the adsorbed amount of CH_4 molecules increases, which suggests that there is inhomogeneity in the adsorption sites on the surface of the material. Notably, the heat of adsorption of all the samples was between 15 and 22 kJ/mol, indicating that these adsorbents have low heat of adsorption and low energy consumption during the adsorption cycle, which is favorable for multiple recycling.

In order to evaluate the regeneration performance of S_3Y_6-800 in practical applications, five CH_4 adsorption–desorption cycling experiments were carried out at 298 K and 1 bar. The experimental results are shown in Figure 9. After five cycles, the adsorption performance of the sample only decreased by 2.04%, indicating its excellent regeneration capability.

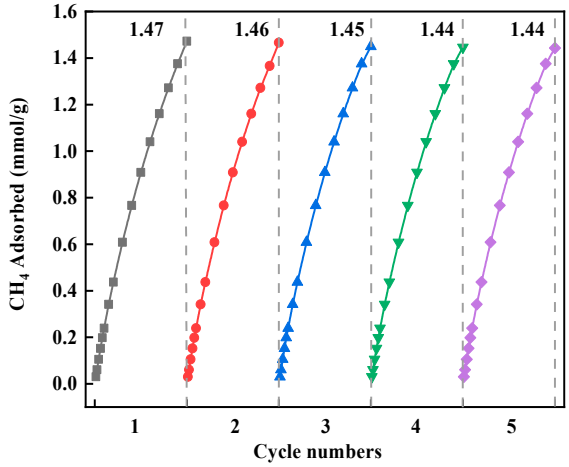


Figure 9. Adsorption cycle stability of S_3Y_6-800.

3.4.3. Dynamic Adsorption of CH_4/N_2 Gas Mixtures

To simulate the adsorption properties of porous carbon in real industrial applications, the penetration curves were measured using a homemade fixed-bed apparatus. Under the experimental conditions (10 mL/min flow rate and a CH_4 to N_2 ratio of 1:1), the results in Figure 10 reveal that N_2 breakthrough occurred earlier than CH_4 for all samples, indicating weak interactions between N_2 and the adsorbent. In the early stage of adsorption, CH_4 molecules preferentially occupied the active sites, leading to the transient penetration of N_2, creating a "roll-up" effect. This competitive adsorption phenomenon occurs because methane's stronger interaction with the adsorbent displaces nitrogen, resulting in methane surpassing nitrogen's exit concentration [8]. Specifically, the temporal order of the breakthrough of CH_4 by the porous carbon material is $S_3Y_6-800 > S_3Y_6-900 > S_3Y_6-700$, and this pattern is consistent with the trend in CH_4 adsorption capacity. Among them, the breakthrough time of S_3Y_6-800 was 420 s, which was significantly longer than that of other samples. This excellent performance can be attributed to its optimal 0.5–0.7 nm narrow microporous volume providing more highly active adsorption sites, which enhances the trapping capacity of CH_4 molecules, and the abundance of nitrogen–oxygen functional groups that increase surface polarity and reactivity, enhancing CH_4 molecule

adsorption and immobilization. These properties not only prolonged the residence time of CH_4 molecules in the adsorbent, but also enhanced the overall adsorption performance.

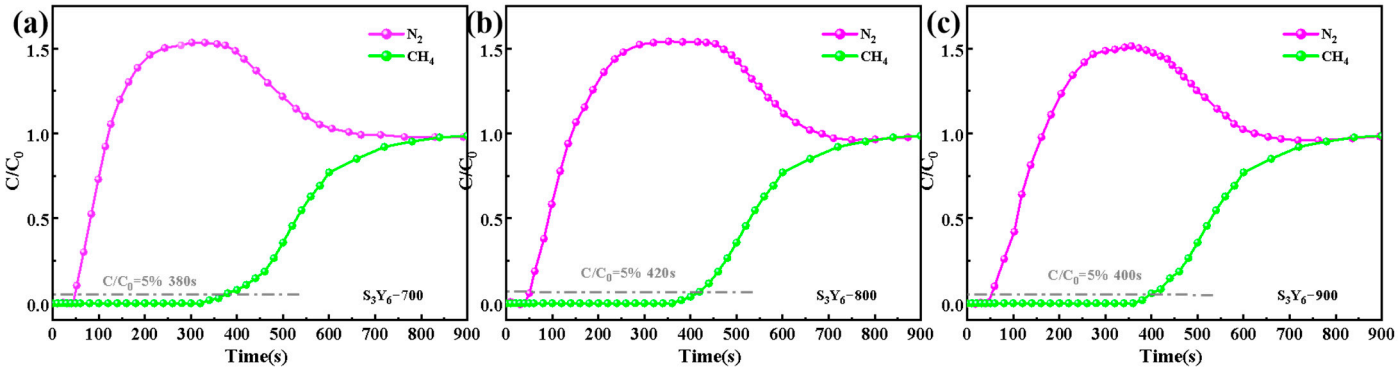


Figure 10. Dynamic permeation curves of samples (**a**) S_3Y_6-700, (**b**) S_3Y_6-800, (**c**) S_3Y_6-900 at CH_4/N_2 (50/50).

3.5. Adsorption Isotherm Fitting

To further investigate the adsorption behavior of S_3Y_6-800 towards CH_4 molecules, its adsorption isotherm at 298 K was fitted using the Langmuir, Freundlich, and Toth models. The results are shown in Figure 11, with the fitting parameters listed in Table 7. All three models demonstrated excellent fitting results, with R^2 values greater than 0.99, indicating a high degree of consistency in the fitted data. Specifically, S_3Y_6-800 exhibits an $R_L < 1$, indicating that the material has good CH_4 adsorption properties. In the Freundlich model, the isotherm constant (K_F) represents the adsorption capacity, while the n value reflects adsorption strength. The n value of 1.299 (>1) suggests that the adsorption process is primarily physical, and the inhomogeneity factor (1/n) of 0.77 further indicates surface inhomogeneity, due to the uneven distribution of micropores or surface functional groups. The Toth model provided the most accurate fit for the adsorption isotherm. The Toth model's inhomogeneous factor (n_T) of 1.1981 indicates nonhomogeneous adsorption on sub-monolayer, where the surface is not entirely homogeneous. When $n_T = 1$, the adsorbent surface is considered homogeneous. The R^2 value of the Toth model (0.9999) demonstrates an extremely high fitting accuracy, suggesting that it provides the most precise description of the adsorption process. According to the R^2 evaluation, the adsorption isotherm fitting followed this order: Toth model (R^2 = 0.9999) > Langmuir model (R^2 = 0.9998) > Freundlich model (R^2 = 0.9985). In conclusion, the Toth model more accurately describes the CH_4 adsorption isotherm of S_3Y_6-800 at 298 K, with the adsorption process consistent with the microporous-filled sub-monolayer coverage mechanism.

3.6. Discussion of the Cost and Scalability of the Process

The proposed method for preparing high-performance porous carbon materials using in situ nitrogen doping combined with K_2CO_3 activation offers several significant advantages in terms of cost-effectiveness and scalability. One of the key benefits lies in the choice of raw materials. By utilizing corn protein powder as a natural nitrogen source, which is inexpensive, widely available, and low in environmental impact, we significantly reduced raw material procurement costs compared to traditional nitrogen sources like ammonia or urea. Additionally, the self-doping nitrogen technology employed in this process eliminates the need for costly chemical additives, streamlining the production process and reducing equipment investments. The use of K_2CO_3 as an activator further contributes to cost reduction by lowering the activation temperature and minimizing energy consumption. This environmentally friendly activator is not only cost-effective but

also helps decrease the overall production costs of the carbon materials. Furthermore, by utilizing agricultural wastes such as corn protein powder and pine shavings, this method promotes effective resource utilization, reducing both the cost of raw materials and the need for waste treatment.

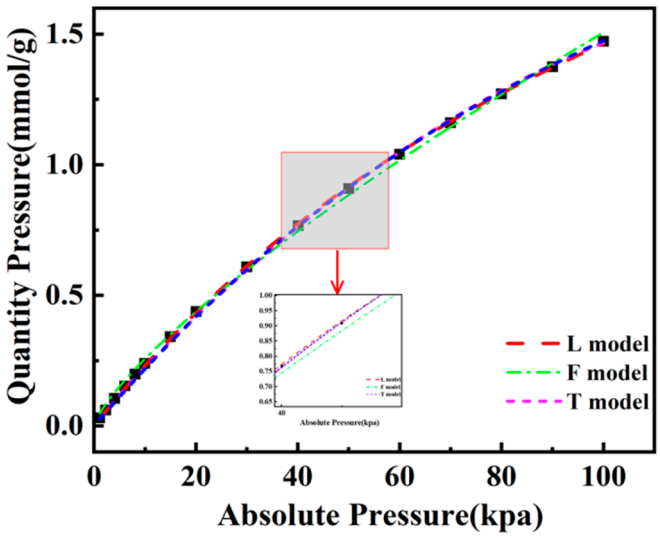


Figure 11. Fitting of adsorption isotherm mode.

Table 7. Adsorption models and parameters.

Model	Nonlinear Equation (Math.)	Parameters	S_3Y_6-800
Langmuir	$q = \frac{Q_O K_L P_e}{1+K_L P_e}$	Q_0	3.6245
		K_L	0.0068
		R^2	0.9998
Freundlich	$q = K_F {P_e}^{1/n}$	K_F	0.0436
		n	1.2999
		R^2	0.9985
Toth	$q = \frac{q_m K_T P_e}{\left[1+\left(K_T P_e^{n_T}\right)\right]^{1/n_T}}$	q_m	8.4862
		K_T	0.0027
		n_T	1.1987
		R^2	0.9999

Scalability is another significant advantage of this process. The choice of widely accessible raw materials, such as corn protein powder and pine wood chips, ensures that the process can be easily adapted for large-scale production. The mild conditions and low activation temperatures associated with K_2CO_3 activation make the process feasible across different production scales, from small batch development to large-scale industrial implementation. The potential for scaling up is further supported by the fact that the raw materials are readily available in agricultural production, facilitating consistent supply.

Finally, the process aligns with sustainable development goals by minimizing environmental impact and promoting a circular economy. By converting agricultural waste into high-value carbon materials, this method not only reduces resource waste but also encourages green transformation in industrial processes. The combination of cost-effective raw materials, simplified production methods, and environmentally friendly technologies makes this process both economically viable and scalable for industrial applications.

4. Conclusions

In this study, we successfully synthesized a series of nitrogen-doped porous carbons through in situ nitrogen doping combined with K_2CO_3 activation. The effects of nitrogen

doping ratio and activation temperature on the porous carbon structure and adsorption properties were systematically examined. The results highlighted that in situ nitrogen doping significantly altered the pore structure, promoting the formation of narrow micropores (0.5–0.7 nm), which are crucial for efficient CH_4 adsorption. Additionally, the introduction of nitrogen and oxygen functional groups, such as N-5, N-6, C-O, and COOH, played a critical role in enhancing the adsorption capacity of the carbon materials. From an operational perspective, the methane adsorption performance was found to be strongly linked to the narrow microporous volume, indicating that optimizing the pore size distribution can significantly improve the efficiency of CH_4/N_2 separation. The results of the thermodynamic analysis, which revealed that methane adsorption is an exothermic physical process with moderate heat of adsorption (15–22 kJ/mol), suggest that these nitrogen-doped porous carbons are highly effective for CH_4 enrichment under ambient conditions. Furthermore, the dynamic breakthrough experiments confirmed that the nitrogen-doped porous carbon materials were capable of efficiently separating methane from nitrogen, a crucial task for improving the quality and economic viability of coalbed methane (CBM) utilization. These findings have important implications for operational practices in the CBM industry. The development of nitrogen-doped porous carbons with tunable pore structures offers a promising approach to enhancing the efficiency of methane separation, addressing key challenges related to CBM exploitation. This study's environmentally friendly and mild preparation method not only facilitates waste utilization but also holds potential for reducing operational costs, making it a viable alternative to traditional, more energy-intensive gas separation technologies. The results underscore the practicality of this approach for large-scale applications, contributing to both environmental sustainability and the economic optimization of CBM production.

Supplementary Materials: The following supporting information can be downloaded at: https://www.mdpi.com/article/10.3390/separations12020042/s1, Figure S1: CH_4/N_2 Breakthrough experimental equipment test diagrams. Table S1: Carbon material yield. Figure S2: Sample S_3Y_6-800.

Author Contributions: Investigation, visualization, writing—original draft preparation, H.W.; conceptualization, methodology, writing—review and editing, project administration, Y.Z.; methodology, investigation, data curation, H.L.; data curation, project administration, Q.W.; conceptualization, resources, Z.S.; writing—review and editing, supervision, G.Z. All authors have read and agreed to the published version of the manuscript.

Funding: This work was supported by the National Science Foundation of Shanxi Province of China (202303021211034 and 202403021212041), the National Natural Science Foundation of China (21805203), and the Lvliang Key R&D of University-Local Cooperation (2022XDHZ06).

Data Availability Statement: Data are contained within the article.

Acknowledgments: We thank Jiangfeng Yang (Shanxi Key Laboratory of Gas Energy Efficient and Clean Utilization, Taiyuan University of Technology) for kindly providing guidance on the test analysis.

Conflicts of Interest: Author Zhihong Shang is employed by Jinneng Holding Group Co., Ltd., Shanxi, China. The remaining authors declare that the research was conducted in the absence of any commercial or financial relationships that could be construed as potential conflicts of interest.

References

1. Zhu, K.; Zhao, Y.; Xu, X. Measuring the natural gas supply security performance of China's natural gas suppliers: A comprehensive framework using FAHP-Entropy-PROOTHEE method. *J. Clean. Prod.* **2022**, *345*, 131093. [CrossRef]
2. Zheng, F.; Chen, L.; Chen, R.; Zhang, Z.; Yang, Q.; Yang, Y.; Bao, Z. A robust two–dimensional layered metal–organic framework for efficient separation of methane from nitrogen. *Sep. Purif. Technol.* **2022**, *281*, 119911. [CrossRef]

3. Liu, Y.; Xu, Q.; Chen, L.; Song, C.; Yang, Q.; Zhang, Z. Hydrogen-bonded metal-nucleobase frameworks for highly selective capture of ethane/propane from methane and methane/nitrogen separation. *Nano Res.* **2022**, *15*, 7695–7702. [CrossRef]
4. Hu, G.; Zhao, Q.; Tao, L.; Xiao, P.; Webley, P.A.; Li, K.G. Enrichment of low grade CH_4 from N_2/CH_4 mixtures using vacuum swing adsorption with activated carbon. *Chem. Eng. Sci.* **2021**, *229*, 116152. [CrossRef]
5. Huang, B.; Zhu, L.; Du, Z.; Anjum, A.W.; Li, X.; Du, S. Highly efficient ethylene/ethane separation via molecular sieving using chitosan-derived ultramicroporous carbon. *Sep. Purif. Technol.* **2024**, *333*, 125862. [CrossRef]
6. Tang, X.; Bai, X.; Wang, Y.; Yang, X.; Li, X.; Li, J.; Yang, J. Optimized mass transfer of PHI-type zeolite for nitrogen/methane sieve separation. *Chem. Eng. J.* **2024**, *495*, 153630. [CrossRef]
7. Wang, J.; Ying, Y.; Guo, P.; Liu, D.; Zhang, W.; Yang, Q. Fabrication of Hofmann-type metal-organic framework based mixed-matrix membranes for efficient CH_4/N_2 separation. *J. Membr. Sci.* **2025**, *713*, 123387. [CrossRef]
8. Wang, S.M.; Wu, P.C.; Fu, J.W.; Yang, Q.Y. Heteroatom-doped porous carbon microspheres with ultramicropores for efficient CH_4/N_2 separation with ultra-high CH_4 uptake. *Sep. Purif. Technol.* **2021**, *274*, 119121. [CrossRef]
9. Huang, J.; Bai, J.; Demir, M.; Hu, X.; Jiang, Z.; Wang, L. Efficient N-doped porous carbonaceous CO_2 adsorbents derived from commercial urea-formaldehyde resin. *Energy Fuels* **2022**, *36*, 5825–5832. [CrossRef]
10. Sher, F.; Iqbal, S.Z.; Albazzaz, S.; Ali, U.; Mortari, D.A.; Rashid, T. Development of biomass derived highly porous fast adsorbents for post-combustion CO_2 capture. *Fuel* **2020**, *282*, 118506. [CrossRef]
11. Zheng, Y.; Li, Q.; Yuan, C.; Tao, Q.; Zhao, Y.; Zhang, G.; Liu, J. Influence of temperature on adsorption selectivity: Coal-based activated carbon for CH_4 enrichment from coal mine methane. *Powder Technol.* **2019**, *347*, 42–49. [CrossRef]
12. Zhang, Y.; Zhao, Y.P.; Qiu, L.L.; Xiao, J.; Wu, F.P.; Cao, J.P.; Liu, F.J. Insights into the KOH activation parameters in the preparation of corncob-based microporous carbon for high-performance supercapacitors. *Diam. Relat. Mater.* **2022**, *129*, 109331. [CrossRef]
13. Andia, J.-M.; Larrea, A.; Salcedo, J.; Reyes, J.; Lopez, L.; Yokoyama, L. Synthesis and characterization of chemically activated carbon from Passiflora ligularis, Inga feuilleei and native plants of South America. *J. Environ. Chem. Eng.* **2020**, *8*, 103892. [CrossRef]
14. Bicil, Z.; Dogan, M. Characterization of activated carbons prepared from almond shells and their hydrogen storage properties. *Energy Fuels* **2021**, *35*, 10227–10240. [CrossRef]
15. Khuong, D.A.; Trinh, K.T.; Nakaoka, Y.; Tsubota, T.; Tashima, D.; Nguyen, H.N.; Tanaka, D. The investigation of activated carbon by K_2CO_3 activation: Micropores-and macropores-dominated structure. *Chemosphere* **2022**, *299*, 134365. [CrossRef]
16. Jia, J.; Song, H.; Jia, P.; Li, B. Adsorption mechanism of $CO_2/CH_4/N_2$ by the synergistic effect of N/S-doped and functional groups in coal at different temperatures and pressures. *Arab. J. Chem.* **2023**, *16*, 105333. [CrossRef]
17. Zhang, X.; Tian, J.; Wang, P.; Liu, T.; Ahmad, M.; Zhang, T.; Song, J. Highly-efficient nitrogen self-doped biochar for versatile dyes' removal prepared from soybean cake via a simple dual-templating approach and associated thermodynamics. *J. Clean. Prod.* **2022**, *332*, 130069. [CrossRef]
18. Cheng, B.H.; Tian, K.; Zeng, R.J.; Jiang, H. Preparation of high performance supercapacitor materials by fast pyrolysis of corn gluten meal waste. *Sustain. Energy Fuels* **2017**, *1*, 891–898. [CrossRef]
19. Liu, H.W.; Hu, X.B.; Hao, W.M.; Cui, X.Y.; Chen, W.P. Methane/nitrogen adsorption separation performance of corn starch-doped asphalt-based activated carbon. *J. Funct. Mater.* **2021**, *52*, 10103–10109.
20. Li, Y.; Xu, R.; Wang, B.; Wei, J.; Wang, L.; Shen, M.; Yang, J. Enhanced N-doped porous carbon derived from KOH-activated waste wool: A promising material for selective adsorption of CO_2/CH_4 and CH_4/N_2. *Nanomaterials* **2019**, *9*, 266. [CrossRef]
21. Yuan, D.; Zheng, Y.; Li, Q.; Lin, B.; Zhang, G.; Liu, J. Effects of pore structure of prepared coal-based activated carbons on CH_4 enrichment from low concentration gas by IAST method. *Powder Technol.* **2018**, *333*, 377–384. [CrossRef]
22. Shen, D.; Bülow, M.; Siperstein, F.; Engelhard, M.; Myers, A.L. Comparison of experimental techniques for measuring isosteric heat of adsorption. *Adsorption* **2000**, *6*, 275–286. [CrossRef]
23. Wu, W.; Wu, C.; Liu, J.; Yan, H.; Li, G.; Zhao, Y.; Zhang, G. Synergistic effects of heteroatom doping and narrow micropores on carbon dioxide capture in bamboo shoot shell-based porous carbon. *Sep. Purif. Technol.* **2024**, *339*, 126690. [CrossRef]
24. Yuan, J.; Wang, Y.; Tang, M.; Zhang, Y. Preparation of N, O co-doped carbon nanotubes and activated carbon composites with hierarchical porous structure for CO_2 adsorption by coal pyrolysis. *Fuel* **2023**, *333*, 126465. [CrossRef]
25. Lei, Y.; Zhao, Y.; Lian, H.; Wang, Y.; Xue, X.; Zhang, G.; Zhang, Y. Enhancement of CH_4/N_2 separation capacity of coal-based porous carbons via hydrothermal coupled KOH activation. *J. Environ. Chem. Eng.* **2024**, *12*, 112477. [CrossRef]
26. Guo, Q.; Zhao, Y.; Lei, Y.; Li, G.; He, Y.; Zhang, G.; Li, K. Tuning Lignite Structure via Hydromodification To Promote the Formation of Coal-Based CNTs: Exploration for the Carbon Source of CNTs. *ACS Omega* **2023**, *8*, 25938–25950. [CrossRef] [PubMed]
27. Lv, X.; Zhang, T.; Luo, Y.; Zhang, Y.; Wang, Y.; Zhang, G. Study on carbon nanotubes and activated carbon hybrids by pyrolysis of coal. *J. Anal. Appl. Pyrolysis* **2020**, *146*, 104717. [CrossRef]

28. Wei, T.; Zhang, Q.; Wei, X.; Gao, Y.; Li, H. A Facile and Low-Cost Route to Heteroatom Doped Porous Carbon Derived from Broussonetia Papyrifera Bark with Excellent Supercapacitance and CO_2 Capture Performance. *Sci. Rep.* **2016**, *6*, 22646. [CrossRef] [PubMed]
29. Wang, Y.; Qiu, X.; Zheng, J. Study the mechanism that carbon nanotubes improve thermal stability of polymer composites: An ingenious design idea with coating silica on CNTs and valuable in engineering applications. *Compos. Sci. Technol.* **2018**, *167*, 529–538. [CrossRef]
30. Pan, H.; Zhao, J.; Lin, Q.; Cao, J.; Liu, F.; Zheng, B. Preparation and characterization of activated carbons from bamboo sawdust and its application for CH_4 selectivity adsorption from a CH_4/N_2 System. *Energy Fuels* **2016**, *30*, 10730–10738. [CrossRef]
31. Wang, S.; Zhang, T.; Li, J.; Hua, Y.; Dou, J.; Chen, X.; Li, S. Potassium citrate-derived porous carbon with high CO_2 capture and Congo red adsorption performance. *Environ. Sci. Eur.* **2023**, *35*, 12302. [CrossRef]
32. Ahmed, R.; Liu, G.; Yousaf, B.; Rehman, A.; Munir, M.A.M.; Irshad, S.; Cheema, A.I. Understanding the synergy between N-doped ultra-microporous carbonaceous adsorbent and nitrogen functionalities for high performance of CO_2 sorption. *J. Environ. Chem. Eng.* **2021**, *9*, 104646. [CrossRef]
33. Li, Y.; Zou, B.; Hu, C.; Cao, M. Nitrogen-doped porous carbon nanofiber webs for efficient CO_2 capture and conversion. *Carbon* **2016**, *99*, 79–89. [CrossRef]
34. Pang, R.; Lu, T.; Shao, J.; Wang, L.; Wu, X.; Qian, X.; Hu, X. Highly efficient nitrogen-doped porous carbonaceous CO_2 adsorbents derived from biomass. *Energy Fuels* **2020**, *35*, 1620–1628. [CrossRef]
35. Li, Y.; Xie, J.; Li, Y.; Yang, Y.; Yang, L. Literature data based systems pharmacology uncovers the essence of "body fire" in traditional Chinese medicine: A case by Huang-Lian-Jie-Du-Tang. *J. Ethnopharmacol.* **2019**, *237*, 266–285. [CrossRef]
36. Li, Q.; Hou, Y.; Han, X.; Wang, J.; Liu, Y.; Xiang, N.; Huang, Z. Promotional effect of cyclic desulfurization and regeneration for selective catalytic reduction of NO by NH_3 over activated carbon. *J. Clean. Prod.* **2020**, *249*, 119392. [CrossRef]
37. Liu, B.; Li, H.; Ma, X.; Chen, R.; Wang, S.; Li, L. The synergistic effect of oxygen-containing functional groups on CO_2 adsorption by the glucose–potassium citrate-derived activated carbon. *R. Soc. Chem. Adv.* **2018**, *8*, 38965–38973. [CrossRef] [PubMed]
38. Ma, X.; Fang, M.; Liu, B.; Chen, R.; Shi, R.; Wu, Q.; Li, L. Urea-assisted synthesis of biomass-based hierarchical porous carbons for the light hydrocarbons adsorption and separation. *Chem. Eng. J.* **2022**, *428*, 130985. [CrossRef]
39. Tagliabue, M.; Farrusseng, D.; Valencia, S.; Aguado, S.; Ravon, U.; Rizzo, C.; Mirodatos, C. Natural gas treating by selective adsorption: Material science and chemical engineering interplay. *Chem. Eng. J.* **2009**, *155*, 553–566. [CrossRef]
40. Cui, H.; Xu, J.; Shi, J.; You, S.; Zhang, C.; Yan, N.; Chen, G. Evaluation of different potassium salts as activators for hierarchically porous carbons and their applications in CO_2 adsorption. *J. Colloid Interface Sci.* **2021**, *583*, 40–49. [CrossRef]
41. Li, Y.; Wang, S.; Wang, B.; Wang, Y.; Wei, J. Sustainable biomass glucose-derived porous carbon spheres with high nitrogen doping: As a promising adsorbent for $CO_2/CH_4/N_2$ Adsorptive Separation. *Nanomaterials* **2020**, *10*, 174. [CrossRef] [PubMed]
42. Wang, Q.; Yu, Y.; Li, Y.; Min, X.; Zhang, J.; Sun, T. Methane separation and capture from nitrogen rich gases by selective adsorption in microporous materials: A review. *Sep. Purif. Technol.* **2022**, *283*, 120206. [CrossRef]
43. Cui, H.; Xu, J.; Shi, J.; Yan, N.; Zhang, C.; You, S. Oxamic acid potassium salt as a novel and bifunctional activator for the preparation of N-doped carbonaceous CO_2 adsorbents. *J. CO2 Util.* **2022**, *64*, 102198. [CrossRef]

Disclaimer/Publisher's Note: The statements, opinions and data contained in all publications are solely those of the individual author(s) and contributor(s) and not of MDPI and/or the editor(s). MDPI and/or the editor(s) disclaim responsibility for any injury to people or property resulting from any ideas, methods, instructions or products referred to in the content.